Accepted Manuscript

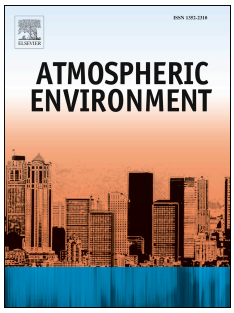

Effect of oligomerization reactions of criegee intermediate with organic acid/peroxy radical on secondary organic aerosol formation from isoprene ozonolysis

Long Chen, Yu Huang, Yonggang Xue, Junji Cao, Wenliang Wang

PII: S1352-2310(18)30378-9

DOI: 10.1016/j.atmosenv.2018.06.001

Reference: AEA 16059

To appear in: *Atmospheric Environment*

Received Date: 11 February 2018

Revised Date: 29 May 2018

Accepted Date: 1 June 2018

Please cite this article as: Chen, L., Huang, Y., Xue, Y., Cao, J., Wang, W., Effect of oligomerization reactions of criegee intermediate with organic acid/peroxy radical on secondary organic aerosol formation from isoprene ozonolysis, *Atmospheric Environment* (2018), doi: 10.1016/j.atmosenv.2018.06.001.

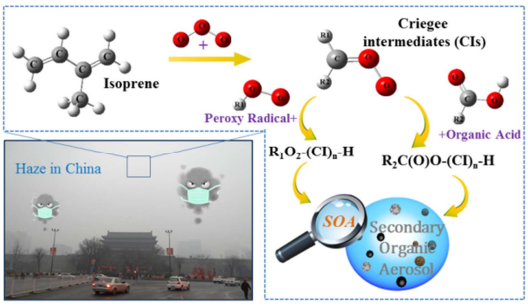

Criegee intermediates generated from isoprene ozonolysis can react with organic acid/peroxy radical leading to SOA.

Effect of Oligomerization Reactions of Criegee Intermediate with Organic Acid/Peroxy Radical on Secondary Organic Aerosol Formation from Isoprene Ozonolysis

Long Chen [a, b], Yu Huang [a, b, *], Yonggang Xue [a, b], Junji Cao [a,b, *], Wenliang Wang [c]

[a] *Key Lab of Aerosol Chemistry & Physics, Institute of Earth Environment, Chinese Academy of Sciences, Xi'an, Shaanxi, 710061, China*

[b] *State Key Laboratory of Loess and Quaternary Geology, Institute of Earth Environment, Chinese Academy of Sciences, Xi'an 710061, China*

[c] *School of Chemistry and Chemical Engineering, Key Laboratory for Macromolecular Science of Shaanxi Province, Shaanxi Normal University, Xi'an, Shaanxi, 710119, China*

Submitted to *Atmospheric Environment*

*Corresponding author:

Prof. Yu Huang, E-mail address: huangyu@ieecas.cn

Prof. Junji Cao, E-mail address: cao@loess.llqg.ac.cn

Tel: + 86-29-62336261, Fax: + 86-29-62336261.

Abstract:

Secondary organic aerosols (SOA) can have significant effects on atmospheric chemistry, human health and climate forcing, but their formation mechanisms via Criegee chemistry are still poorly understood. Here we present a comprehensive theoretical investigation on the oligomerization reaction of stabilized Criegee intermediates (SCIs) with organic acid/peroxy radical by using *ab initio* quantum-chemical methodologies. Our results show that the ozonolysis of isoprene easily leads to a series of C3 and C4 stable CIs due to its larger exothermicity and spontaneity. The formed SCIs have two isomers: *syn*- and *anti*-, and *anti*- is more stable in energy than that of *syn*- by about 2-5 kcal·mol^{-1}. The barrier heights of oligomerization reactions are very sensitive to the size and structure of functional groups near the central carbon atom site, indicating they can be tuned by the substitutions. Reaction between SCIs and peroxy radical contributes significantly to the formation of oligomer which is the dominant component of SOA. However, the reaction between SCIs and organic acid plays an important role in aerosol nucleation in some regions where high SCI and low H_2O concentrations occur such as in terrestrial equatorial area. Such knowledge should be useful for understanding the mechanism of SOA formation from the alkenes ozonolysis and for developing atmospheric chemistry models.

Keywords: Isoprene ozonolysis; Criegee intermediates; Oligomerization reactions, Reaction mechanisms; Rate coefficients;

1. Introduction

Haze pollution in China is extremely severe during cold winter periods, threatening the health of ~800 million people living in a region of ~1.3 million km^2 (Huang et al., 2014; Cheng et al., 2016). Long-term exposure to polluted air is linked to respiratory infections, chronic bronchitis, emphysema, heart attack and lung cancer (Lelieveld et al., 2017; Liu et al., 2015; Jimenez et al., 2009). The persistent and severe haze pollution event is driven to a large extent by secondary organic aerosol (SOA) formation, which accounts for 33-77% and 44-71% of the mass concentrations of $PM_{2.5}$ (particulate matter with a diameter of less than 2.5 μm) and organic aerosol (OA) (Huang et al., 2014).

Of all of the volatile organic compounds (VOCs) emitted into the atmosphere, isoprene is the largest atmospheric emission of non-methane hydrocarbons(~ 600 Tg/year) (Kumar et al., 2015; Sakamoto et al., 2017; Sakamoto et al., 2001; Piletic et al., 2017; Guenther et al., 2006). Isoprene oxidation in the atmosphere is thought to be responsible for a large amount of SOA production at the regional and global scales (Inomata et al., 2014). Reactions involving the hydroxyl (OH) and nitrate (NO_3) radicals are major pathways of oxidation during both the day and the night (Xu et al., 2014; Ng et al., 2008). In addition, the ozonolysis of isoprene is also the main atmospheric oxidation pathway in the troposphere (Sakamoto et al., 2017; Nguyen et al., 2016). It should be noted that the ozone reaction occurs throughout the day and globally removes ~ 10% of isoprene (Nguyen et al., 2016; Johnson et al., 2008). At emission levels of 600 Tg/year, even minor sink of isoprene may exert major effects on atmospheric pollutant concentrations (Piletic et al., 2017). Moreover, the ozone reaction can couple with other oxidation processes in the atmosphere (Inomata et al., 2014). Therefore, we think that it is important to understand the mechanism of SOA formation in the gas-phase ozonolysis of isoprene.

Gas-phase ozonolysis of isoprene generates a series of carbonyl oxides (also called Criegee intermediates (CIs)), as reactive intermediates. Nascent CIs accompany with the considerable amount of vibrational energy owing to the formation of primary

ozonide (POZ) with strong exothermicity, which proceed via collisional energy transfer processes generating stabilized Criegee intermediates (SCIs) (Cabezas et al., 2017) that undergo unimolecular decomposition to yield OH radical (Chen et al., 2016; Kidwell et al., 2016) or occur bimolecular reactions with atmospheric species such as water vapour (Berndt et al., 2015; Berndt et al., 2014; Chen et al., 2016), peroxy radical (Long et al., 2011) and organic acid (Nguyen et al., 2016) to generate oligomers. These oligomers have sufficiently low saturated vapour pressures and thus contribute to the tropospheric budgets of hydroxyl radicals (Kidwell et al., 2016), organic acids (Foreman et al., 2016) and SOA (Zhang et al., 2015).

Formic acid (HC(O)OH) as a proxy for the organic acids, which is largely emitted from tropical forest and is contributed significantly to the formation of acid rain that damage forest and farm plants (Stavrakou et al., 2012). Typical atmospheric concentration of formic acid is in the range of ~ 1-10 ppbv (Tobias et al., 2001; Vereecken et al., 2014). Methyl peroxy radical (CH_3O_2) as a prototypical example of the alkyl peroxy radicals (RO_2) that is the most important oxidant in the VOCs with a global production (~ 2,500 Tg/year) primarily due to the daytime oxidation of methane by the OH radical in the presence of O_2 (Müller et al., 2016; Chameides et al., 1973; Assaf et al., 2017). The bimolecular reactions of SCIs with organic acid and peroxy radical are one of the dominant chemical sinks of carbonyl oxides and lead to oligomeric hydroperoxides that have sufficiently low saturated vapour pressures (~ 10^{-3}-10^{-4} Torr) to potentially significant contribution to SOA formation (Inomata et al., 2014). In addition, there are significant literatures suggesting that Criegee chemistry at the air-water interface (Zhu et al., 2016; Kumar et al., 2017; Zhong et al., 2017; Enami et al., 2017; Zhong et al., 2018) follows both concerted and stepwise mechanisms with former being the dominant mechanistic pathway.

The experimental studies have suggested that oligomers containing a SCI as the chain units are expected to participate in secondary organic aerosol (SOA) formation from alkenes ozonolysis (Inomata et al., 2014; Sadezky et al., 2008; Sakamoto et al., 2013). Sakamoto et al. (Sakamoto et al., 2013) conducted the ethylene ozonolysis in laboratory experiments using a Teflon bag reactor, and found that CH_2OO can

produce oligomers followed by SOA formation via reactions with formic acid and hydroperoxides in the gaseous phase. Sadezky et al. (Sadezky et al., 2008) proposed that the mechanism of SCI reaction with peroxy radical (R_1O_2) leading to oligomer R_1O_2-$(SCI)_n$-H that is involving initiation by the reaction of SCI with a R_1O_2 radical, sequential addition of SCIs, and the chain termination by reaction with the HO_2 radical. This oligomer formation mechanism is written as follows:

$$R_1O_2 + SCI \rightarrow R_1O_2\text{-}SCI \quad (1)$$

$$R_1O_2\text{-}SCI + (n\text{-}1)SCI \rightarrow R_1O_2\text{-}(SCI)_{n\text{-}1}\text{-}SCI \quad (2)$$

$$R_1O_2\text{-}(SCI)_{n\text{-}1}\text{-}SCI + HO_2 \rightarrow R_1O_2\text{-}(SCI)_n\text{-}H + O_2 \quad (3)$$

Similar to the work mentioned above, Zhao et al. (Zhao et al., 2015) concluded the same from the ozonolysis experiment of trans-3-hexene in a flow reactor and in static chambers in the absence and presence of an OH or SCI scavenger at 295 ± 1 K. They found that oligomers having SCI as the chain unit are the dominant components of SOA, and the sequential addition of C_2H_5CHOO to R_1O_2 radical is a favorable reaction mode. The bimolecular reaction with organic acid can provide a new pathway in which these acids are converted to low-volatility oligomeric hydroperoxides and thus contribute to the formation of SOA in the troposphere (Sakamoto et al., 2017; Welz et al., 2014).

$$R_2C(O)OH + SCI \rightarrow R_2C(O)O\text{-}SCI\text{-}H \quad (4)$$

$$R_2C(O)O\text{-}SCI\text{-}H + (n\text{-}1)SCI \rightarrow R_2C(O)O\text{-}(SCI)_n\text{-}H \quad (5)$$

The theoretical investigation mentioned above mainly focuses on small carbonyl oxides systems (e.g. CH_2OO, *syn*-/*anti*-CH_3CHOO and $(CH_3)_2COO$) (Zhao et al., 2017; Johnson et al., 2001; Long et al., 2009), but little study has been done on the reactivity of C3 and C4 SCIs as formed in isoprene ozonolysis toward organic acid and peroxy radical as far as we know. It is because their direct experimental identification and characterization have proven extremely difficult due to their complicated structure, high reactivity and short lifetime (Vereecken et al., 2012). Moreover, the ozonolysis experiments cannot distinguish the *syn*- and

anti-conformers of SCIs, which have completely distinct reactivity in the formation of oligomer (Zhao et al., 2017). To the best of our knowledge, both theoretical studies on the reaction mechanism between CH_2OO and CH_3OO have been reported by Vereecken et al. (Vereecken et al., 2012) and Anglada et al. (Anglada et al., 2013) by means of different quantum-mechanical methods. They found that this reaction proceeds initially by the formation of a strong pre-reactive complex followed by a submerged barrier for subsequent addition of CH_3OO terminal oxygen atom to the CH_2OO central carbon atom, leading to a larger peroxy radical CH_3OOCH_2OO. Zhao et al. (Zhao et al., 2017) concluded the same from the reactions of hydroxyl-substituted alkylperoxy radicals with SCIs, that is, the addition reaction is a favorable reaction mode for SOA formation. The main goal of this work is to explore the detailed mechanism and related rate coefficient of the oligomerization reaction of SCI with organic acid/peroxy radical leading to the formation of SOA from the ozonolysis of isoprene. We will further evaluate the atmospheric implications of these oligomerization reactions using kinetic modeling. The result insights can promote a better understanding of the atmospheric formation of SOA from unsaturated hydrocarbons ozonolysis.

2. Computational details

All quantum chemical calculations reported here are executed using the Gaussian 09 program suite (Frisch et al., 2009). Lee et al. (Lee et al., 2013) investigated the transient infrared absorption spectrum of CH_2OO, and observed that the vibrational frequencies are more consistent with a zwitterion rather than a diradical structure. Miliordos et al. (Miliordos et al., 2016) and Chen et al. (Chen et al., 2016) concluded the same by the quantum-chemical calculations that CH_2OO is indeed a closed-shell system, with its ground state minimum geometry best represented as the $H_2C{=}O^{\delta+}\text{-}O^{\delta-}$ zwitterion. Previous theoretical studies have shown that the coupled-cluster//DFT level of theory can provide reasonable results for describing the geometries, zero-point energies (ZPE), and frequencies for Criegee chemistry (Chen et al., 2016; Nguyen et al., 2015; Su et al., 2014; Buras et al., 2014; Raghunath et al., 2017; Chen

et al., 2017). Thus, in the present study, the geometries of all the stationary points on the potential energy surfaces are fully optimized using the B3LYP functional (Zheng et al., 2009) along with the 6-311+G(2df,2p) basis set (Anglada et al., 2011). The Grimme's dispersion correction method is employed to describe medium range correlation effects (Grimme et al., 2010). Harmonic vibrational frequencies are performed to ascertain the nature of local minima (NIMAG = 0) and saddle point (NIMAG = 1). A scale factor of 0.986 (Buras et al., 2014) is applied to scale all the B3LYP-D3/6-311+G(2df,2p) frequencies to account for the thermodynamic contribution to the Gibbs free energy and enthalpy at 298.15 K and 1 atm. The connectivity between the two energy minimum points is established by intrinsic reaction coordinate (IRC) calculations (Fukui et al., 1981; Page et al., 1988; Gonzalez et al., 1989; Gonzalez et al., 1990). On the basis of the B3LYP-D3 optimized geometries, the single point energies are calculated at the CCSD(T)/6-311+G(2df,2p) level of theory (Mendes et al., 2013). The coupled-cluster approach CCSD(T) involves single and double substitutions with a perturbative treatment of triple excitations (Mendes et al., 2013), which is reliable to characterize electronic energies in the present study because T_1 diagnostics are all less than the critical value 0.02 (Mendes et al., 2013). Finally, the kinetic parameter is calculated using conventional transition state theory (TST) with an one-dimensional Eckart tunneling correction factor (Eckart et al., 1930; Johnston et al., 1962; Garrett et al., 1979) and the thermodynamic equivalent form is employed (Zhao et al., 2017).

$$k^{\mathrm{TST}}(T) = \sigma \frac{k_{\mathrm{b}}T}{h}\left(\frac{\mathrm{R}T}{P^{0}}\right)^{\Delta n}\exp\left(\frac{-\Delta G^{\dagger}(T)}{k_{\mathrm{b}}T}\right) \tag{6}$$

where $\Delta G^{\dagger}(T)$ is activation Gibbs free energy; σ is reaction symmetry number; k_{b} is the Boltzmann's constant; T is the temperature in Kelvin; h is the Planck's constants; Δn= 1 and Δn = 0 stand for the bimolecular and unimolecular reactions (Zhao et al., 2017). The rate coefficients at the temperatures 273-400 K are calculated by implementing KiSThelP program (Canneaux et al., 2014).

3. Results and discussion

3.1 The isoprene ozonolysis

Previous experimental studies have shown that organic peroxy radicals (RO_2) generated from the isoprene photooxidation primarily react with HO_2 radical leading to the formation of SOA under low-NO_x conditions, while it mainly reacts through multiple pathways, including with NO, NO_2, and HO_2 forming SOA under high-NO_x conditions (Xu et al., 2014). The reactions of RO_2 with HO_2 and NO_x produce low volatile species via fragmentation of the resultant RO radical (Kroll et al., 2008). In the present study, the dihydroxy-epoxides (IEPOX) and hydroxymethyl-methyl-α-lactone (HMML) pathways of isoprene SOA formation are taken into consideration, and are compared with the channels of isoprene ozonolysis. Shown in Fig. S1 is a simplified scheme of the IEPOXs and HMML pathways. The corresponding potential energy surfaces are constructed in Figs. S2 and S3 using the CCSD(T)//B3LYP-D3/6-311+G(2df,2p) energies.

As shown in Fig. S2, the IEPOX pathways are strongly exothermic and spontaneous, signifying that they are feasible thermochemically under atmospheric conditions. Isoprene oxidation begins with the addition of OH radical to the C=C bond, sequential reactions with $^3O_2$, HO_2 and OH radicals forming IEPOX under low-NO_x conditions. The rate-limiting step of IEPOX pathways is the TS_R2 with the barrier of 6.7 kcal·mol^{-1}. From Fig. S3, one can see that the RO_2 radical (S-3) chemistry is more complex in the presence of NO_x as compared with the presence of HO_2 radical. The HMML pathways start with the addition reaction of isoprene with OH radical, sequential reactions through multiple pathways, including $^3O_2$ and NO, forming MACR. Then, the continued reaction of MACR proceeds mainly through MAC + OH/$^3O_2$/HO_2 pathways to form HMML. The rate-determining step of HMML pathways is the TS_R5 with the barrier of 30.6 kcal·mol^{-1}, in good agreement with the value of 31.0 kcal·mol^{-1} reported by Piletic and coworker (Piletic et al., 2017). Although the barrier of the rate-determining step TS_R5 is high, the large exothermicity of the HMML pathways may provide sufficient energies to overcome such an activation energy. Thus, the IEPOX pathways under low-NO_x conditions and

HMML pathways under high-NO_x conditions are the important processes for isoprene SOA formation.

As shown in Fig. 1, the barriers of isoprene ozonolysis are 7.6 (R1) and 6.5 (R4) kcal·mol^{-1} and the large exothermicity ~ 40 kcal·mol^{-1}. They are large exothermicity and low barrier, suggesting that the ozonolysis of isoprene in the atmosphere are feasible both thermochemically and dynamically. By comparing the barriers and exothermicity of the ozone reactions, IEPOX and HMML pathways, one can find that the isoprene ozonolysis has some competition in the formation of SOA. This conclusion implies again that it is essential to investigate the mechanism and kinetic of SOA formation from isoprene ozonolysis. A simplified mechanism of isoprene ozonolysis is drawn in Scheme 1. Optimized structures of all the stationary points on the potential energy surfaces are illustrated in Figs. S4-S7 with available experimental and theoretical values for comparison. For the species CH_2OO, CH_2O, HC(O)OH, H_2O and O_3, the mean absolute deviations (MAD) between the calculated values and the experimental ones are 0.007 Å (bond lengths) and 0.9° (bond angles). The largest deviations are 0.015 Å for O-O bond in O_3 molecule and 1.6° for ∠H-C-O angle in CH_2OO intermediate and ∠O-O-O angle in O_3 molecule. In view of the above, we feel that the B3LYP-D3 functional applied herein is accurate enough for a realistic description of the title reaction system from both equilibrium geometries and characterize mechanisms. Additionally, the rotational constants of CH_2OO are also listed in Table S1, agree satisfactorily with the experimental and theoretical reports (Chen et al., 2017). The relative energies plus ZPE (ΔE_R), enthalpies (ΔH_R), free energies (ΔG_R), activation energies ($\Delta E_a^{\#}$) and free energies ($\Delta G_a^{\#}$) of elementary reaction involved in the isoprene ozonolysis are presented in Table S2.

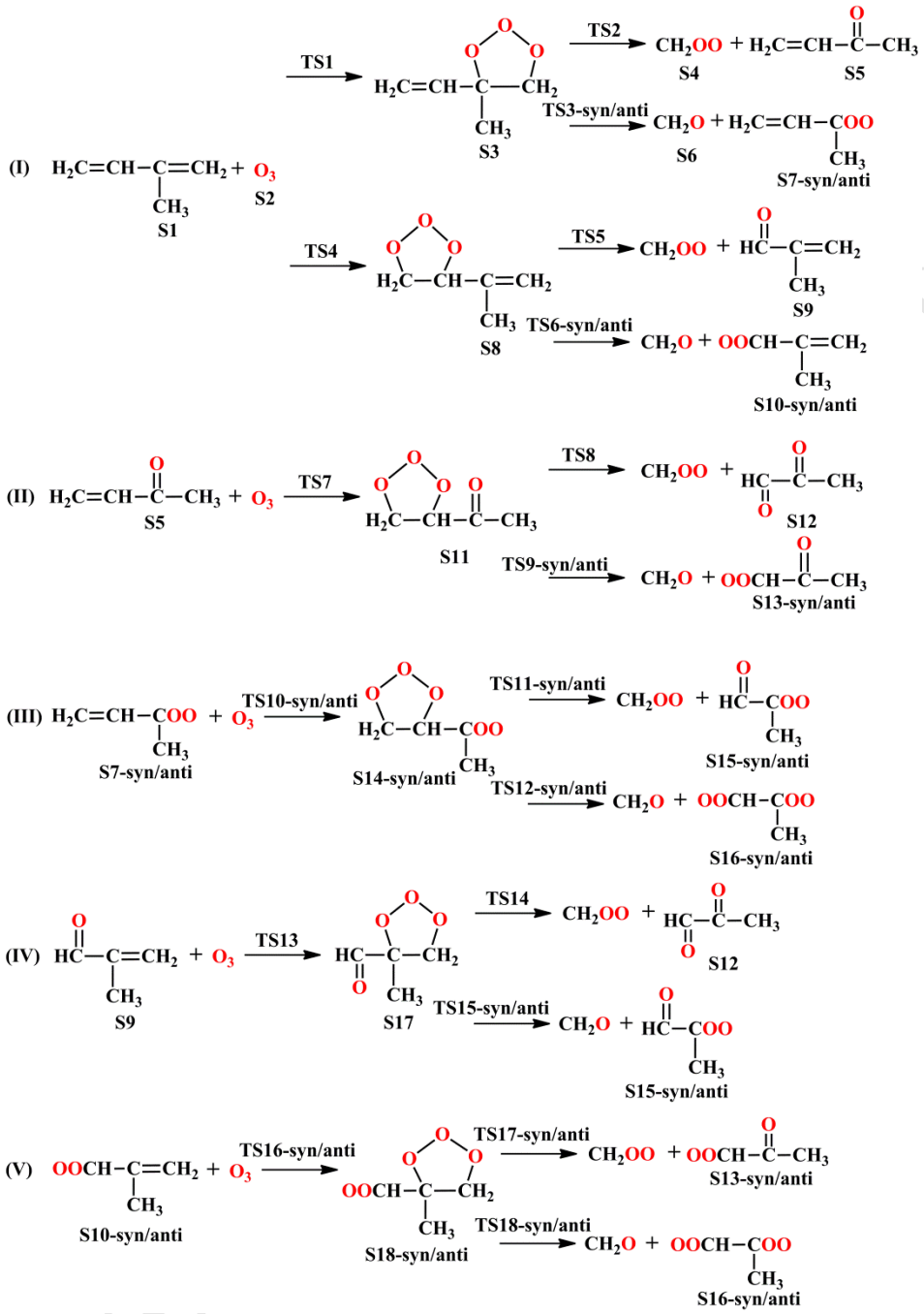

Scheme 1 Brief description for isoprene ozonolysis

Shown in Fig. 1 is the relative energy diagram of isoprene ozonolysis according to the energies obtained with the CCSD(T)//B3LYP-D3/6-311+G(2df,2p) method. In this figure, the differences between the relative free energies and the electronic energies for the majority of stationary points are significant due to the large contributions from entropy effects. Similar behaviors are also observed in the ozonolysis of other alkenes and oligomerization reactions of Criegee intermediates with organic acid and peroxy radical (see Figs. 2-6). Thus, in the present work, unless

mentioned otherwise, the free energy barriers ($\Delta G_a^{\#}$) are applied to discuss in the subsequent analysis.

There are two channels (R1 and R4) that have been observed in the bimolecular reaction of isoprene with ozone: (i) the cycloaddition of O_3 on the C=C bond (B1) leading to CH_2=CHC(CH_3)CH_2O_3 (S3), (ii) the cycloaddition of O_3 across the C=C bond (B2) forming CH_2=C(CH_3)$CHCH_2O_3$ (S8). Both pathways proceed initially by the formations of strong pre-reactive complexes IM1 and IM4, of 6.6 and 7.3 kcal·mol^{-1} stability. Then the complexes transform subsequently to the ozonides S3 and S8 with the barriers of 7.6 (TS1) and 6.5 (TS4) kcal·mol^{-1} and with exothermicity ~40 kcal·mol^{-1}. The result shows that the addition of ozone on a C=C bond (B1) forming S8 is more preferable than on another C=C bond (B2) producing S3. The reason can be attributed to steric repulsion between methyl group and ozone. The addition reactions R1 and R4 are large exothermicity and low barrier, suggesting that the ozonolysis of isoprene are feasible both thermochemically and dynamically. Because of their large exothermicity, the ozonolysis reactions leave a significant amount of internal energy in the newly formed SCIs, leading to rapid bimolecular decay (Taatjes et al., 2017).

The decomposition of ozonide S3 generated from channel R1 has three pathways (R2, R3-*syn* and R3-*anti*), namely the homolytic cleavage of C-C and O-O bonds leading to the formations of CH_2OO + CH_2=CHC(O)CH_3 (S4 + S5) and CH_2O + CH_2=CHC(CH_3)OO (S6 + S7-*syn*/*anti*). The Criegee intermediate S7 exists in two conformations: *syn* and *anti*. The -CH=CH_2 group is on the same side with respect to the O-O bond in a S7-*syn*, whereas it is on the opposite side in a S7-*anti* (see Fig. S4). Calculations show that *anti*- is more favorable in energy than *syn*- by about 2.5 kcal·mol^{-1} due to hyperconjugative interaction between the -CH=CH_2 and carbonyl groups. The product complexes IM2, IM3-*syn* and IM3-*anti* are formed occurring before the corresponding final products. The binding energies are 6.2, 3.0 and 3.5 kcal·mol^{-1} energetically higher than the separated products, and -10.1, -16.5 and -18.5 kcal·mol^{-1} more stable than the reactant S3. The corresponding transition states TS2, TS3-*syn* and TS3-*anti* are predicted to lie -22.7, -24.8 and -25.8 kcal·mol^{-1},

respectively, below the energies of the initial reactants isoprene and ozone, and 17.5, 15.4 and 14.4 kcal·mol^{-1} above the energy of reactant S3. The result shows that the most favourable channel is the reaction R3-*anti* due to its lower barrier. Similar conclusion is also drawn in the calculated results of electronic energies.

Equivalent to the decomposition of ozonide S3, the ozonide S8 formed by channel R4 also has three decomposition pathways (R5, R6-*syn* and R6-*anti*). It can either lead to CH_2OO + $HC(O)C(CH_3)=CH_2$ (S4 + S9), or produce CH_2O + $CH_2=C(CH_3)CHOO$ (S6 + S10-*syn*/*anti*). The barriers of these three pathways are 15.8(R5), 19.1(R6-*syn*) and 15.7(R6-*anti*) kcal·mol^{-1} and the large exothermicity -15.3(R5), -14.0(R6-*syn*) and -16.5(R6-*anti*) kcal·mol^{-1}. The result shows that the channel R6-*syn* is less competitive compared to other two pathways on both thermochemically and dynamically. Moreover, the barriers of the S10-*syn* reactions with HC(O)OH, CH_3OO and H_2O are higher than that of the S10-*anti* system (see Fig. 5-6, S8-S9 and S11), indicating the *anti*-conformer is substantially more reactive toward HC(O)OH, CH_3OO and H_2O than is *syn*-conformer in the atmosphere. Similar conclusion has been obtained from the *syn*-/*anti*-CH_3CHOO reactions with atmospheric species such as alkylperoxy radicals, water and SO_2 (Vereecken et al., 2014; Zhao et al., 2017; Lin et al., 2016; Huang et al., 2012; Taatjes et al., 2013; Anglada et al., 2016).

Similar to the ozonolysis of isoprene, its decomposition products $CH_2=CHC(O)CH_3$ (S5) and $CH_2=CHC(CH_3)OO$ (S7-*syn*/*anti*) also react with ozone leading to a set of C3 SCIs. The PES is constructed in Fig. 2 using the CCSD(T)//B3LYP-D3/6-311+G(2df,2p) energies.

In Fig. 2(a), the initial association of $CH_2=CHC(O)CH_3$ (S5) and O_3 yields a strong pre-reactive complex IM7, followed by it transforms to a excited ozonide $CH_3C(O)CHCH_2O_3$ (S11) with internal energy ~ 40 kcal·mol^{-1}. Then, the ozonide S11 dissociates into CH_2OO + $CH_3C(O)C(O)H$ (S4 + S12) with its transition state TS8 located 14.6 kcal·mol^{-1}, or decomposes into CH_2O + $CH_3C(O)CHOO$ (S6 + S13-*syn*/*anti*) with their transition states TS9-*syn* and TS9-*anti* located 19.7 and 18.3 kcal·mol^{-1} above that of the energy of reactant S11. The result shows that the former

reaction R8 is more advantaged than that of the latter two pathways R9-*syn* and R9-*anti*, but its thermodynamically unfavorable compare to the R9-*anti*.

As shown in Fig. 2(b), the S7-*anti* is more stable in energy than S7-*syn* by about 2.5 kcal·mol^{-1} due to hyperconjugative effect. The addition reaction between CH_2=CHC(CH_3)OO (S7-*syn*) and O_3 starts with the formation of pre-reactive complex IM10-*syn* in the entrance channel followed by the above energy of 6.5 kcal·mol^{-1}. Then the IM10-*syn* transforms to ozonide S14-*syn* with the barrier of 8.0 kcal·mol^{-1} (TS10-*syn*) and with exothermicity ~ 38 kcal·mol^{-1}. Because of its large exothermicity, it may provide sufficient energies to overcome the barriers of secondary reactions. It can either generate CH_2OO + HC(O)C(CH_3)OO (S4 + S15-*syn*) with the barrier of 14.7 kcal·mol^{-1}, or produce CH_2O + OOCHC(CH_3)OO (S6 + S16-*syn*) with the barrier of 20.1 kcal·mol^{-1}. It can be found that the former pathway is obviously preferable due to its lower barrier. Similar conclusion is also obtained from the S7-*anti* + O_3 reaction system. The detailed mechanism of S7-*anti* + O_3 reaction is almost the same as S7-*syn* + O_3 system. In order to avoid redundancy, we do not repeat them here in detail.

The adducts CH_2=C(CH_3)C(O)H (S9) and CH_2=C(CH_3)CHOO (S10-*syn*/*anti*) generated from channels R5 and R6-*syn*/*anti* can further react with O_3 leading to various types of C3 SCIs, which have enough high reactivity to contribute the formation of SOA. The PES of ozone reactions with S9 and S10-*syn*/*anti* is constructed in Fig. 3 using above mentioned method. The mechanistic details of S9 + O_3 and S10-*syn*/*anti* + O_3 systems are quite similar to that of the S5 + O_3 and S7-*syn*/*anti* + O_3 systems. Thus, in order to avoid redundancy, we will not be discussed in detail for these addition reactions.

3.2 The addition reactions of SCIs with organic acid

The SCIs generated from isoprene ozonolysis can help us to better understanding the Criegee chemistry occurring in the forest and in urban environments. The formed SCIs have two conformers, *syn*- and *anti*-, depending upon the relative spatial orientation of the substituent group with respect to the O-O bond. From the results

pointed out in the previous paragraph, we have concluded that the stability of *anti*-SCI is much larger than that of *syn*-SCI and is judiciously selected to study their oligomerization reactions. The PESs of oligomerization reactions of *syn*-SCIs with organic acid and peroxy radical are only displayed in Figs. S8 and S9, and do not discuss them in detail. In the present study, we concentrate on the oligomerization reactions of *anti*-SCIs with organic acid and peroxy radical, and compare to their reactions with water vapour. The optimized geometries and NPA atomic charges of *anti*-SCIs are displayed in Fig. 4.

The bimolecular reaction of *anti*-SCI with HC(O)OH can provide a new pathway in which HC(O)OH is converted to low volatility and highly oxidized oligomer and thus contribute to the formation of SOA (Sakamoto et al., 2017). The addition of HC(O)OH across the -COO moiety of *anti*-SCI occurs in a concerted manner, which leads to the exothermic formation of hydroperoxyalkyl carboxylate (Nguyen et al., 2016; Aplincourt et al., 2000). The corresponding PES is shown in Fig. 5.

As can be seen from Fig. 5, the addition reactions of *anti*-SCIs with HC(O)OH are strongly exothermic and spontaneous, revealing that they are accessible pathway thermochemically. These reactions would first go through the barrierless formations of pre-reactive complexes (IM19-IM24-*anti*) followed by the submerged energies. These complexes are -1.7, -4.3, -5.9, -0.9, -2.5 and -2.1 kcal·mol^{-1} energetically with respect to the respective reactants. Then, the energized complexes convert rapidly to the products hydroperoxyalkyl carboxylates. The barrier heights predict TS19, 20-*anti*, 21-*anti*, 22-*anti*, 23-*anti* and 24-*anti* to lie 9.9, 11.8, 5.1, 11.2, 12.2 and 12.6 kcal·mol^{-1}, respectively, above the energies of the separate reactants *anti*-SCIs and HC(O)OH, and 10.6, 16.1, 11.0, 12.1, 14.9 and 14.7 kcal·mol^{-1} above the energies of the respective pre-reactive complexes. The result shows that the energetically most favourable channels are CH_2OO + HC(O)OH (R19) and S10-*anti* + HC(O)OH systems (R21-*anti*), and the barrier heights strongly depend on the structure of reactants. The conclusion is further supported by the previous literatures that the reactivity of carbonyl oxide strongly depends on the nature and position of substituents (Zhao et al., 2017; Anglada et al., 2011). For CH_2OO + HC(O)OH

reaction, the computed barrier is 10.6 kcal·mol^{-1}, in good agreement with theoretical calculations at higher level (10.5 kcal·mol^{-1} at the CBS-QB3 level of theory) (Long et al., 2009). The -CH=CH_2 (S7-*anti*), -C(O)H (S15-*anti*) and -CHOO (S16-*anti*) groups on *β*-hydrogen atom and methyl group on *α*-hydrogen atom lead to significantly higher barriers with respect to the reaction of parent carbonyl oxide. This phenomenon can be explained by the hyperconjugative interaction between the methyl group and the COO carbon (Anglada et al., 2011; Zhao et al., 2017).

To gain deeper insights into the effect of ionic property on the reaction barrier, we examine the NPA charges using the natural bond orbital (NBO) method. And the result is displayed in Fig. 4. In this figure, the charge of CH_2OO central carbon atom C1 is positive (0.157 e) while its terminal oxygen atom O1 is negative (-0.417 e), indicating that CH_2OO intermediate indeed is a zwitterion. The methyl substituent in the *α*-position induces the accumulation of C1 atom charge with respect to the parent carbonyl oxide, which leads to the barriers of S7-/S15-/S16-*anti* + HC(O)OH systems increasing by ~ 4.0 kcal·mol^{-1}. This is because the electron donor character of methyl group hinders the nucleophilic attack of the oxygen atom of formic acid.

3.3 The addition reactions of SCIs with peroxy radical

The addition reaction of SCI with CH_3O_2 radical leads to peroxide-substituted alkyl peroxy radical and opening the possibility for the formation of SOA (Sadezky et al., 2008). The detailed mechanism involves that the terminal oxygen atom of CH_3O_2 radical directly binds to the SCI carbon atom forming oligomer CH_3OO-(SCI). The analysis of the wave functions shows that the formation of the newly C-O bond occurs by interaction of the unpaired electron of the CH_3O_2 radical with the two electrons on the 2p and 3p molecular orbitals of SCI. The PES of *anti*-SCIs reactions with CH_3O_2 radical is shown in Fig. 6.

As seen from Fig. 6, the bimolecular reactions of *anti*-SCIs with CH_3O_2 are also strongly exothermic and spontaneous. These reactions start with the formation of pre-reactive loosely bound complexes in which the two components are held together by van der Waals interactions between the terminal oxygen atom of CH_3O_2 radical

and the central carbon atom of *anti*-SCIs, and by hydrogen bonds between one of the hydrogen atoms of CH_3O_2 radical and the *anti*-SCIs terminal oxygen atom. These complexes IM25-IM30-*anti* are stabilized relative to the respective reactants from 2.6 to 3.8 kcal·mol^{-1}, suggesting that the CH_3O_2 radical is tied up in these complexes. They convert rapidly to the respective products via a series of transition states with moderate barriers. The barrier heights of these six addition reactions are decreased in the order of 11.1 (TS29-*anti*) > 11.0 (TS27-*anti*) > 9.7 (TS26-*anti*) > 8.2 (TS30-*anti*) > 7.1 (TS28-*anti*) > 1.7 (TS25) kcal·mol^{-1}, indicating that the favorable channel is the CH_2OO + CH_3OO reaction and the barrier heights vary considerably with size and structure of *anti*-SCIs and explain in terms of conjugative, hyperconjugative, and steric interactions (Anglada et al., 2011). Compared to the *anti*-SCIs + HC(O)OH reaction mode, it can be found that the barriers for *anti*-CI + CH_3OO systems are comparatively low. The result shows that the reactivity of *anti*-SCIs toward CH_3OO is the best in this title reaction system.

3.4 Kinetics and implication in atmospheric chemistry

The kinetic parameters are calculated using conventional transition state theory (TST), with tunneling correction factor estimated assuming an asymmetric Eckart potential (Chen et al., 2016; Zhang et al., 2012). Fig. 7 presents the Arrhenius plots of rate coefficients for the reactions of *anti*-SCIs with HC(O)OH and CH_3OO in the temperature range from 273 to 400 K.

As shown in Fig. 7(a), the rate coefficients of *anti*-SCIs + HC(O)OH reactions increase with rising temperature, and the differences raise up to four orders of magnitude depending on the carbonyl oxide. The result indicates that the reactivity of *anti*-SCIs toward formic acid strongly depends on size, position and structure of substituents. The substituted carbonyl oxides toward formic acid have low reactivity with respect to the parent carbonyl oxide, and they will be able to react with other atmospheric species contributing to the formation of SOA. For example, for CH_2OO + HC(O)OH reaction, the computed rate coefficient is 3.5×10^{-15} cm^3 molecule^{-1} s^{-1}, in good agreement with the upper limit experimental value 1.0×10^{-14} cm^3 molecule^{-1}

s^{-1} from Johnson et al. via adding organic acid to the O_3/2-methylbut-2-ene system (Johnson et al., 2001). In Fig. 7(b), the rate coefficients of *anti*-SCIs + CH_3OO reactions decrease with increasing temperature, and they exhibit a slightly negative T-dependency. The kinetic parameters vary considerably with size and location of substituents, which is further supported by the recent literature reports (Anglada et al., 2013; Anglada et al., 2011). The rate coefficients of *anti*-SCIs + CH_3OO reactions are much higher than that of the *anti*-SCIs + HC(O)OH systems, indicating that the reactivity of *anti*-SCIs toward CH_3OO radical is the best.

Considering the Criegee-water reaction is the most plausible reaction in the troposphere, it would be interesting to examine whether the reactions between *anti*-SCIs and HC(O)OH/CH_3O_2 can compete well with the reactions between *anti*-SCIs and H_2O under atmospheric conditions. This is because water vapor is the third most abundant molecule existing in the Earth's atmosphere ([H_2O] ≈ 7.0×10^{17} molecules cm^{-3}) (Zhang et al., 2014; Zhang et al., 2015) and one of the dominant chemical sinks for SCIs is the reaction with water vapour (Chao et al., 2015; Smith et al., 2015). Although the concentration of water in the troposphere is several orders of magnitude larger than organic acid and peroxy radical, the larger rate coefficient could partly compensate the low concentrations of HC(O)OH and CH_3OO radical. The PESs and kinetic parameters of *anti*-SCIs reactions with water vapour are displayed in Figs. S11 and S12, respectively. As shown in Fig. S12, the differences in the rate coefficient of different substituted carbonyl oxides raise up to six orders of magnitude with respect to the parent carbonyl oxide. The result indicates that the substituted carbonyl oxides toward water vapour have low reactivity and have much longer lifetime in the troposphere, and reactions with other atmospheric species such as organic acid and peroxy radical may become important to contribute to the formation of SOA. By comparing the reaction barriers and rate coefficients of *anti*-SCIs reactions with H_2O, HC(O)OH and CH_3OO, one can find that the *anti*-SCIs + CH_3OO reactions exhibit more obvious advantage than that of the analogous *anti*-SCIs + H_2O/HC(O)OH reactions. Though the barriers of *anti*-SCIs + HC(O)OH reactions are generally equal to the *anti*-SCIs + H_2O systems, these reactions are mediated by

pre-reaction complexes that are more stable than separated reactants. Therefore, the *anti*-SCIs + HC(O)OH reactions could be potentially able to compete with the reaction of water vapour in terrestrial equatorial areas and in some northern high latitude locations (Welz et al., 2014). As a result, the *anti*-SCIs + CH_3OO reactions make a major contribution to the formation and growth of SOA under highly humid conditions, while the *anti*-SCIs + HC(O)OH reactions play an important role in aerosol nucleation in some regions, where high CI concentrations and low H_2O concentrations occur such as northern high latitude.

4. Conclusion

The mechanisms and kinetics of oligomerization reactions of Criegee intermediates with organic acid/peroxy radical from the ozonolysis of isoprene are studied using *ab initio* quantum-chemical methodologies in conjunction with statistical theory calculations. The main conclusions are summarized as follows:

(a) The SCIs generated from the isoprene ozonolysis have two isomers: *syn*- and *anti*-, and the *anti*- is more stable in energy than that of *syn*- by about 2-5 $kcal \cdot mol^{-1}$.

(b) The barrier heights of oligomerization reactions of SCIs with organic acid and peroxy radical strongly depend on the size, position and structure of substituents.

(c) The rate coefficients of *anti*-SCIs + HC(O)OH reactions increase with rising temperature, whereas the rate coefficients of *anti*-SCIs + CH_3O_2 systems decrease with increasing temperature. The rate coefficients of these bimolecular reactions vary considerably with size and structure of the SCIs.

(d) Reactions between SCIs and peroxy radical contribute significantly to the formation of SOA under the condition of high relative humidity, while the reactions between SCIs and organic acid play an important role in aerosol nucleation in terrestrial equatorial areas.

Acknowledgments

This work was supported by the National Key Research and Development

Program of China (2016YFA0203000) and the National Science Foundation of China (Nos. 41401567, 41573138 and 21473108). It was also partially supported by the Key Project of International Coperation of the Chinese Academy of Sciences (GJHZ1543) and the Research Grants Council of Hong Kong (PolyU 152083/14E), Open foundation of State Key Laboratory of Loess and Quaternary Geology (SKLLQG1627), and Shaanxi Province Postdoctoral Science Foundation funded project (No. 2017BSHEDZZ62).

References

Huang, R. J., Zhang, Y., Bozzetti, C., Ho, K. F., Cao, J. J., Han, Y., Daellenbach, K. R., Slowik, J. G., Platt, S. M., Canonaco, F., Zotter, P., Wolf, R., Pieber, S. M., Bruns, E. A., Crippa, M., Ciarelli, G., Piazzalunga, A., Schwikowski, M., Abbaszade, G., Schnelle-Kreis, J., Zimmermann, R., An, Z., Szidat, S., Baltensperger, U., Haddad, I. E., Prévôt, A. S. H., 2014. High secondary aerosol contribution to particulate pollution during haze events in China. Nature 514 (7521), 218-222.

Cheng, Y., Zheng, G., Wei, C., Mu, Q., Zheng, B., Wang, Z., Gao, M., Zhang, Q., He, K., Carmichael, G., Pöschl, U., Su, H., 2016. Reactive nitrogen chemistry in aerosol water as a source of sulfate during haze events in China. Sci. Adv. 2 (12), e1601530.

Lelieveld, J., Pöschl, U., 2017. Chemists can help to solve the air-pollution health crisis. Nature 551 (7680), 291-293.

Liu, J., Fang, S., Wang, Z., Yi, W., Tao, F. M., Liu, J. Y., 2015. Hydrolysis of sulfur dioxide in small clusters of sulfuric acid: mechanistic and kinetic study. Environ. Sci. Technol. 49 (22), 13112-13120.

Jimenez, J. L., Canagaratna, M. R., Donahue, N. M., Prevot, A. S. H., Zhang, Q., 2009. Evolution of organic aerosols in the atmosphere. Science 326 (5959), 1525-1529.

Kumar, M., Francisco, J. S., 2015. Red-light-induced decomposition of an organic peroxy radical: a new source of the HO_2 radical. Angew. Chem. Int. Ed. 54 (52), 15711-15714.

Sakamoto, Y., Yajima, R., Inomata, S., Hirokawa, J., 2017. Water vapour effects on secondary organic aerosol formation in isoprene ozonolysis. Phys. Chem. Chem. Phys. 19 (4), 3165-3175.

Tobias, H. J., Ziemann, P. J., 2001. Kinetics of the gas-phase reactions of alcohols, aldehydes, carboxylic acids, and water with the C13 stabilized Criegee intermediate formed from ozonolysis of 1-tetradecene. J. Phys. Chem. A 105 (25), 6129-6135.

Piletic, I. R., Edney, E.O., Bartolotti, L. J., 2017. Barrierless reactions with loose transition states govern the yields and lifetimes of organic nitrates derived from isoprene. J. Phys. Chem. A 121 (43), 8306-8321.

Guenther, A., Karl, T., Harley, P., Wiedinmyer, C., Palmer, P. I., Geron, C., 2006. Estimates of global terrestrial isoprene emissions using MEGAN (Model of Emissions of Gases and Aerosols from Nature). Atmos. Chem. Phys. 6 (11), 3181-3210.

Inomata, S., Sato, K., Hirokawa, J., Sakamoto, Yosuke., Tanimoto, H., Okumura, M., Tohno, Susumu., Imamura, T., 2014. Analysis of secondary organic aerosols from ozonolysis of

isoprene by proton transfer reaction mass spectrometry. Atmos. Environ. 97 (97), 397-405.

Xu, L., Kollman, M. S., Song, C., Shilling, J. E., Ng, N. L., 2014. Effects of NOx on the volatility of secondary organic aerosol from isoprene photooxidation. Environ. Sci. Technol. 48 (4), 2253-2262.

Ng, N. L., Kwan, A. J., Surratt, J. D., Chan, A. W. H., Chhabra, P. S., Sorooshian, A., Pye, H. O. T., Crounse, J. D., Wennberg, P. O., Flagan, R. C., Seinfeld, J. H., 2008. Secondary organic aerosol (SOA) formation from reaction of isoprene with nitrate radicals (NO_3). Atmos. Chem. Phys. 8 (14), 4117-4140.

Nguyen, T. B., Tyndall, G. S., Crounse, J. D., Teng, A. P., Bates, K. H., Schwantes, R. H., Coggon, M. M., Zhang, L., Feiner, P., Milller, D. O., Skog, K. M., Rivera-Rios, J. C., Dorris, M., Olson, K. F., Koss, A., Wild, R. J., Brown, S. S., Goldstein, A. H., de Gouw, J. A., Brune, W. H., Keutsch, F. N., Seinfeld, J. H., Wennberg, P. O., 2016. Atmospheric fates of Criegee intermediates in the ozonolysis of isoprene. Phys. Chem. Chem. Phys., 18, 10241-10254.

Johnson, D., Marston, G., 2008. The gas-phase ozonolysis of unsaturated volatile organic compounds in the troposphere. Chem. Soc. Rev. 37 (4), 699-716.

Cabezas, C., Endo, Y., 2017. Spectroscopic characterization of the reaction products between Criegee Intermediate CH_2OO and HCl. Chem. Phys. Chem. 18 (14), 1860-1863.

Chen, L., Wang, W. L., Wang, W. N., Liu, Y. L., Liu, F. Y., Liu, N., Wang, B. Z., 2016. Water-catalyzed decomposition of the simplest Criegee intermediate CH_2OO. Theor. Chem. Acc. 135 (5), 131-143.

Kidwell, N. M., Li, H., Wang, X., Bowman, J. M., Lester M. I., 2016. Unimolecular dissociation dynamics of vibrationally activated CH_3CHOO Criegee intermediates to OH radical products. Nat. Chem. 8 (5), 509-514.

Berndt, T., Kaethner, R., Voigtländer, J., Stratmann, F., Pfeifle, M., Reichle, P., Sipilä, M., Kulmala, M., Olzmann, M., 2015. Kinetics of the unimolecular reaction of CH_2OO and the bimolecular reactions with the water monomer, acetaldehyde and acetone under atmospheric conditions. Phys. Chem. Chem. Phys. 17 (30), 19862-19873.

Berndt, T., Voigtländer, J., Stratmann, F., Junninen, H., Mauldin III, R. L., Sipilä, M., Kulmala, M., Herrmann, H., 2014. Competing atmospheric reactions of CH_2OO with SO_2 and water vapour. Phys. Chem. Chem. Phys. 16 (36), 19130-19136.

Chen, L., Wang. W. L., Zhou, L. T., Wang, W. N., Liu, F. Y., Li, C. Y., Lü, J., 2016. Role of water clusters in the reaction of the simplest Criegee intermediate CH_2OO with water vapour. Theor. Chem. Acc. 135 (11), 252-263.

Long, B., Tan, X. F., Long, Z. W., Wang, Y. B., Ren, D. S., Zhang, W. J., 2011. Theoretical studies on reactions of the stabilized H_2COO with HO_2 and the HO_2...H_2O complex. J. Phys. Chem. A 115 (24), 6559-6567.

Foreman, E. S., Kapnas, K. M., Murray, C., 2016. Reactions between Criegee intermediates and the inorganic acids HCl and HNO_3: kinetics and atmospheric implications. Angew. Chem. Int. Ed. 55 (35), 10419-10422.

Zhang, X., McVay, R. C., Huang, D. D., Dalleska, N. F., Aumont, B., Flagan, R. C., Seinfeld, J. H., 2015. Formation and evolution of molecular products in α-pinene secondary organic aerosol. Proc. Natl. Acad. Sci. U.S.A. 112 (46), 14168-14173.

Stavrakou, T., Müller, J. F., Peeters, J., Razavi, A., Clarisse, L., Clerbaux, C., Coheur, P. F., Hurtmans, D., Mazière, M. D., Vigouroux, C., Deutscher, N. M., Griffith, D. W. T., Jones, N., Paton-Walsh, C., 2012. Satellite evidence for a large source of formic acid from boreal and tropical forests. Nature Geosci. 5 (1), 26-30.

Vereecken, L., Harder, H., Novelli, A., 2014. The reactions of Criegee intermediates with alkenes, ozone, and carbonyl oxides. Phys. Chem. Chem. Phys. 16 (9), 4039-4049.

Müller, J. F., Liu, Z., Nguyen, V. S., Stavrakou, T., Harvey, J. N., Peeters, J., 2016. The reaction of methyl peroxy and hydroxyl radicals as a major source of atmospheric methanol. Nat. Commun. 7, 13213-11.

Chameides, W., Walker, J. C. G., 1973. A photochemical theory of tropospheric ozone. J. Geophys. Res. 78 (36), 8751-8760.

Assaf, E., Sheps, L., Whalley, L., Heard, D., Tomas, A., Schoemaecker, C., Fittschen, C., 2017. The reaction between CH_3O_2 and OH radicals: product yields and atmospheric implications. Environ. Sci. Technol. 51 (4), 2170-2177.

Zhu, C., Kumar, M., Zhong, J., Li, L., Francisco, J. S., Zeng, X. C., 2016. New mechanistic pathways for Criegee-water chemistry at the air/water interface. J. Am. Chem. Soc. 138 (35), 11164-11169.

Kumar, M., Zhong, J., Francisco, J. S., Zeng, X. C., 2017. Criegee intermediate-hydrogen sulfide chemistry at the air/water interface. Chem. Sci. 8, 5385-5391.

Zhong, J., Kumar, M., Zhu, C. Q., Francisco, J. S., Zeng, X. C., 2017. Surprising stability of larger Criegee intermediates on aqueous interfaces. Angew. Chem. Int. Ed. 56 (27), 7740-7744.

Enami, S., Colussi, A. J., 2017. Efficient scavenging of Criegee intermediates on water by surface-active cis-pinonic acid. Phys. Chem. Chem. Phys. 19 (26), 17044-17051.

Zhong, J., Kumar, M., Francisco, J. S., Zeng, X. C., 2018. Insight into chemistry on cloud/aerosol water surfaces. Acc. Chem. Res. 51 (5), 1229-1237.

Sadezky, A., Winterhalter, R., Kanawati, B., Römpp, A., Spengler, B., Mellouki, A., Bras, G. L., Chaimbault, P., Moortgat, G. K., 2008. Oligomer formation during gas-phase ozonolysis of small alkenes and enol ethers: new evidence for the central role of the Criegee intermediate as oligomer chain unit. Atmos. Chem. Phys. 8 (10), 2667-2699.

Sakamoto, Y., Inomata, S., Hirokawa, J., 2013. Oligomerization reaction of the Criegee intermediate leads to secondary organic aerosol formation in ethylene ozonolysis. J. Phys. Chem. A 117 (48), 12912-12921.

Zhao, Y., Wingen, L. M., Perraud, V., Greaves, J., Finlayson-Pitts, B. J., 2015. Role of the reaction of stabilized Criegee intermediates with peroxy radicals in particle formation and growth in air. Phys. Chem. Chem. Phys., 17 (19), 12500-12514.

Welz, O., Eskola, A. J., Sheps, L., Rotavera, B., Savee, J. D., Scheer, A. M., Osborn, D. L., Lowe, D., Booth, A. M., Xiao, P., Khan, M. A. H., Percival, C. J., Shallcross, D. E., Taatjes, C. A., 2014. Rate coefficients of C1 and C2 Criegee intermediate reactions with formic and acetic acid near the collision limit: direct kinetics measurements and atmospheric implications. Angew. Chem. Int. Ed. 53 (18), 4547-4550.

Zhao, Q., Liu, F., Wang, W., Li, C., Lu, J., Wang, W., 2017. Reactions between hydroxyl-substituted alkylperoxy radicals and Criegee intermediates: correlations of the electronic characteristics of methyl substituents and the reactivity. Phys. Chem. Chem. Phys. 19 (23), 15073-15083.

Johnson, D., Lewin, A. G., Marston, G., 2001. The effect of Criegee-intermediate scavengers on the OH yield from the reaction of ozone with 2-methylbut-2-ene. J. Phys. Chem. A 105 (13), 2933-2935.

Long, B., Cheng, J. R., Tan, X. F., Zhang, W. J., 2009. Theoretical study on the detailed reaction mechanisms of carbonyl oxide with formic acid. J. Mol. Struct. Theochem. 916 (1), 159-167.

Vereecken, L., Harder, H., Novelli, A., 2012. The reaction of Criegee intermediates with NO, RO_2, and SO_2, and their fate in the atmosphere. Phys. Chem. Chem. Phys. 14 (42), 14682-14695.

Anglada, J. M., Olivella, S., Solé, A., 2013. The reaction of formaldehyde carbonyl oxide with the methyl peroxy radical and its relevance in the chemistry of the atmosphere. Phys. Chem. Chem. Phys. 15 (43), 18921-18933.

Frisch, M. J., Trucks, G. W., Schlegel, H. B., Scuseria, G. E., Robb, M. A., Cheeseman, J. R., Montgomery, J. A. Jr., Vreven, T., Kudin, K. N., Burant, J. C., Millam, J. M., Iyengar, S. S., Tomasi, J., Barone, V., Mennucci. B., Cossi, M., Scalmani, G., Rega, N., Petersson, G. A., Nakatsuji, H., Hada, M., Ehara, M., Toyota, K., Fukuda, R., Hasegawa, J., Ishida, M., Nakajima, T., Honda, Y., Kitao, O., Nakai, H., Klene, M., Li, X., Knox, J. E., Hratchian, H. P., Cross, J. B., Adamo, C., Jaramillo, J., Gomperts, R., Stratmann, R. E., Yazyev, O., Austin, A. J., Cammi, R., Pomelli, C., Ochterski, J. W., Ayala, P. Y., Morokuma, K., Voth, G. A., Salvador, P., Dannenberg, J. J., Zakrzewski, V. G., Dapprich, S., Daniels, A. D., Strain, M. C., Farkas, O., Malick, D. K., Rabuck, A. D., Raghavachari, K., Foresman, J. B., Ortiz, J. V., Cui, Q., Baboul, A. G., Clifford, S., Cioslowski, J., Stefanov, B. B., Liu, G., Liashenko, A., Piskorz, P., Komaromi, I., Martin, R. L., Fox, D. J., Keith, T., Al-Laham, M. A., Peng, C. Y., Nanayakkara, A., Challacombe, M., Gill, P. M. W., Johnson, B., Chen, W., Wong, M. W., Gonzalez, C., Pople, J. A., 2009. Gaussian 09, Revision D.01; Gaussian, Inc.: Wallingford, CT.

Su, Y. T., Huang, Y. H., Witek, H. A., Lee, Y. P., 2013. Infrared absorption spectrum of the simplest Criegee intermediate CH_2OO. Science 340 (6129), 174-176.

Miliordos, E., Xantheas, S. S., 2016. The origin of the reactivity of the Criegee intermediate: implications for atmospheric particle growth. Angew. Chem. Int. Ed. 55 (3), 1015-1019.

Nguyen, T. N., Putikam, R., Lin, M. C., 2015. A novel and facile decay path of Criegee intermediates by intramolecular insertion reactions via roaming transition states. J. Chem. Phys. 142, 124312-6.

Su, Y. T., Lin, H. Y., Putikam, R., Matsui, H., Lin, M. C., Lee, Y. P., 2014. Extremely rapid self-reaction of the simplest Criegee intermediate CH_2OO and its implications in atmospheric chemistry. Nat. Chem. 6 (6), 477-483.

Buras, Z. J., Elsamra, R. M. I., Jalan, A., Middaugh, J. E., Green, W. H., 2014. Direct kinetic measurements of reactions between the simplest Criegee intermediate CH_2OO and alkenes. J. Phys. Chem. A 118 (11), 1997-2006.

Raghunath, P., Lee, Y. P., Lin, M. C., 2017. Computational chemical kinetics for the reaction of Criegee intermediate CH_2OO with HNO_3 and its catalytic conversion to OH and HCO. J. Phys. Chem. A 121 (20), 3871-3878.

Chen, L., Huang, Y., Xue, Y., Cao, J. J., Wang, W., 2017. Competition between HO_2 and H_2O_2 reactions with CH_2OO/*anti*-CH_3CHOO in the oligomer formation: a theoretical

perspective. J. Phys. Chem. A 121 (37), 6981-6991.

Zheng, J., Truhlar, D. G., 2009. Direct dynamics study of hydrogen-transfer isomerization of 1-pentyl and 1-hexyl radicals. J. Phys. Chem. A 113 (43), 11919-11925.

Anglada, J. M., González, J., Torrent-Sucarrat, M., 2011. Effects of the substituents on the reactivity of carbonyl oxides. A theoretical study on the reaction of substituted carbonyl oxides with water. Phys. Chem. Chem. Phys. 13 (28), 13034-13045.

Grimme, S., Antony, J., Ehrlich, S., Krieg, H., 2010. A consistent and accurate ab initio parametrization of density functional dispersion correction (DFT-D) for the 94 elements H-Pu. J. Chem. Phys. 132 (15), 154104-19.

Fukui, K., 1981. The path of chemical reactions - the IRC approach. Acc. Chem. Res. 14 (12), 363-368.

Page, M., Mclver, J. W., 1988. On evaluating the reaction path Hamiltonian. J. Chem. Phys. 88 (2), 922-935.

Gonzalez, C., Schlegel, H. B., 1989. An improved algorithm for reaction path following. J. Chem. Phys. 90 (90), 2154-2161.

Gonzalez, C., Schlegel, H. B., 1990. Reaction path following in mass-weighted internal coordinates. J. Phys. Chem. 94 (14) , 5523-5527.

Mendes, J., Zhou, C. W., Curran, H. J., 2013. Theoretical and kinetic study of the reactions of ketones with HO_2 radicals. Part I: abstraction reaction channels. J. Phys. Chem. A 117 (22), 4515-4525.

Mendes, J., Zhou, C. W., Curran, H. J., 2013. Theoretical and kinetic study of the hydrogen atom abstraction reactions of esters with HO_2 radicals. J. Phys. Chem. A 117 (51), 14006-14018.

Eckart, C., 1930. The penetration of a potential barrier by electrons. Phys. Rev. 35 (11), 1303-1309.

Johnston, H. S., Heicklen, J., 1962. Tunneling corrections for unsymmetrical Eckart potential energy barriers. J. Phys. Chem. 66 (3), 532-533.

Garrett, B. C., Truhlar, D. G., 1979. Semiclassical tunneling calculations. J. Phys. Chem. 83 (22), 2921-2926.

Canneaux, S., Bohr, F., Henon, E., 2014. KiSThelP: A program to predict thermodynamic properties and rate constants from quantum chemistry results. J. Comput. Chem. 35 (1), 82-93.

Kroll, J. H., Seinfeld, J. H., 2008. Chemistry of secondary organic aerosol: Formation and evolution of low-volatility organics in the atmosphere. Atmos. Environ. 42 (16), 3593-3624.

Taatjes, C. A., Liu, F., Rotavera, B., Kumar, M., Caravan, R., Osborn, D. L., Thompson, W. H., Lester, M. I., 2017. Hydroxyacetone production from C3 Criegee intermediates. J. Phys. Chem. A 121 (1), 16-23.

Lin, L. C., Chang, H. T., Chang, C. H., Chao, W., Smith, M. C., Chang, C. H., Lin, J. J., Takahashi, K., 2016. Competition between H_2O and $(H_2O)_2$ reactions with CH_2OO/CH_3CHOO. Phys. Chem. Chem. Phys. 18 (6), 4557-4568.

Huang, H. L., Chao, W., Lin, J. J. M., 2012. Kinetics of a Criegee intermediate that would survive high humidity and may oxidize atmospheric SO_2. Proc. Natl. Acad. Sci. U.S.A. 112 (35), 10857-10862.

Taatjes, C. A., Welz, O., Eskola, A. J., Savee, J. D., Scheer, A. M., Shallcross, D. E., Rotavera, B., Lee,

E. P. F., Dyke, J. M., Mok, D. K. W., Osborn, D. L., Percival, C. J., 2013. Direct measurements of conformer-dependent reactivity of the Criegee intermediate CH_3CHOO. Science,. 340 (6129), 177-180.

Anglada, J. M., Solé, A., 2016. Impact of water dimer on the atmospheric reactivity of carbonyl oxides. Phys.Chem.Chem.Phys. 18 (26), 17698-17712

Aplincourt, P., Ruiz-López, M. F., 2000. Theoretical study of formic acid anhydride formation from carbonyl oxide in the atmosphere. J. Phys. Chem. A 104 (2), 380-388.

Zhao, Q., Wang, W., Liu, F., Lu, J., Wang, W., 2017. Oligomerization reactions for precursors to secondary organic aerosol: Comparison between two formation mechanisms for the oligomeric hydroxyalkyl hydroperoxides. Atmos. Environ. 166, 1-8.

Zhang, P., Wang, W. L., Zhang, T. L., Chen, L., Du, Y. M., Li, C. Y., Lü, J., 2012. Theoretical study on the mechanism and kinetics for the self-reaction of $C_2H_5O_2$ radicals. J. Phys. Chem. A 116 (18), 4610-4620.

Zhang, W., Du, B., Qin, Z., 2014. Catalytic effect of water, formic acid, or sulfuric acid on the reaction of formaldehyde with OH radicals. J. Phys. Chem. A 118 (26), 4797-4807.

Zhang, T., Wang, R., Chen, H., Min, S., Wang, Z., Zhao, C., Xu, Q., Jin, L., Wang, W., Wang, Z., 2015. Can a single water molecule really affect the HO_2 + NO_2 hydrogen abstraction reaction under tropospheric conditions? Phys. Chem. Chem. Phys. 17 (22), 15046-15055.

Chao, W., Hsieh, J. T., Chang, C. H., Lin, J. J. M., 2015. Direct kinetic measurement of the reaction of the simplest Criegee intermediate with water vapor. Science 347 (6223), 751-4.

Smith, M. C., Chang, C. H., Chao, W., Lin, L. C., Takahashi, K., Boering, K. A., Lin, J. J. M., 2015. Strong negative temperature dependence of the simplest Criegee intermediate CH_2OO reaction with water dimer. J. Phys. Chem. Lett. 6 (14) , 2708-2713.

Figure Captions:

Fig. 1. Potential energy surface (ΔG and ΔE (*italic*)) of isoprene ozonolysis at the CCSD(T)//B3LYP-D3/6-311+G(2df,2p) level of theory

Fig. 2. Potential energy surfaces (ΔG and ΔE (*italic*)) of ozonolysis of S5(a) and S7(b) at the CCSD(T)//B3LYP-D3/6-311+G(2df,2p) level of theory

Fig. 3. Potential energy surfaces (ΔG and ΔE (*italic*)) of the ozonolysis of S9(a) and S10(b) at the CCSD(T)//B3LYP-D3/6-311+G(2df,2p) level of theory

Fig. 4. The geometrical parameters (normal) and NPA charges (*italic*) of *anti*-SCIs calculated at the B3LYP-D3/6-311+G(2df,2p) level of theory (α and β stand for the position of substituent group)

Fig. 5. Potential energy surface (ΔG and ΔE (*italic*)) of *anti*-SCIs reactions with HC(O)OH at the CCSD(T)//B3LYP/6-311+G(2df,2p) level of theory

Fig. 6. Potential energy surface (ΔG and ΔE (*italic*)) of *anti*-SCIs reactions with CH_3O_2 at the CCSD(T)//B3LYP-D3/6-311+G(2df,2p) level of theory

Fig. 7. Arrhenius plots of rate coefficients $k(T)$ (cm^3 $molecule^{-1}$ s^{-1}) for *anti*-SCIs + HC(O)OH (a) and *anti*-SCIs + CH_3OO (b) reactions versus $1000/T$ (K^{-1}) at 273-400 K

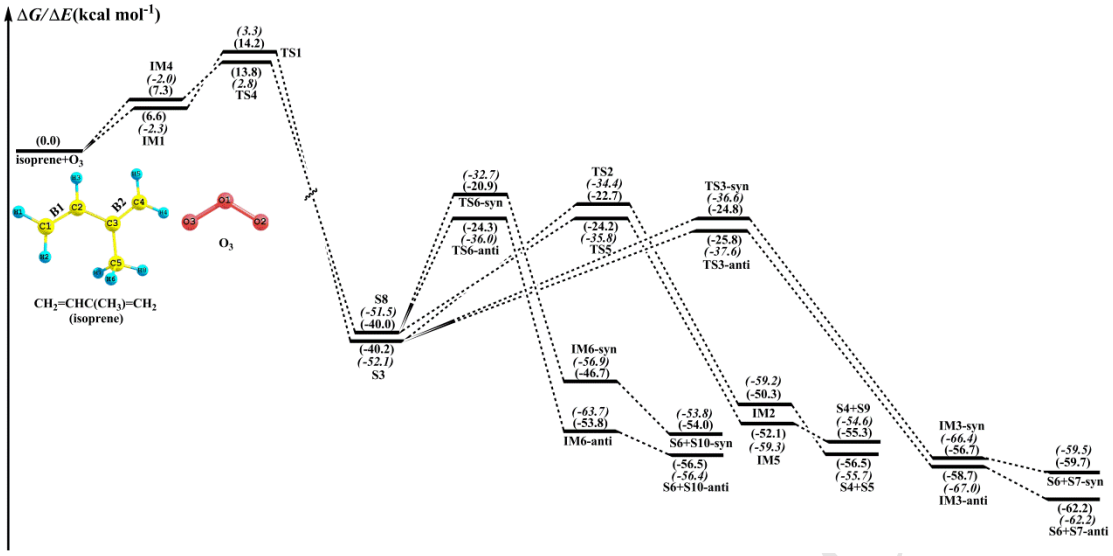

Fig. 1

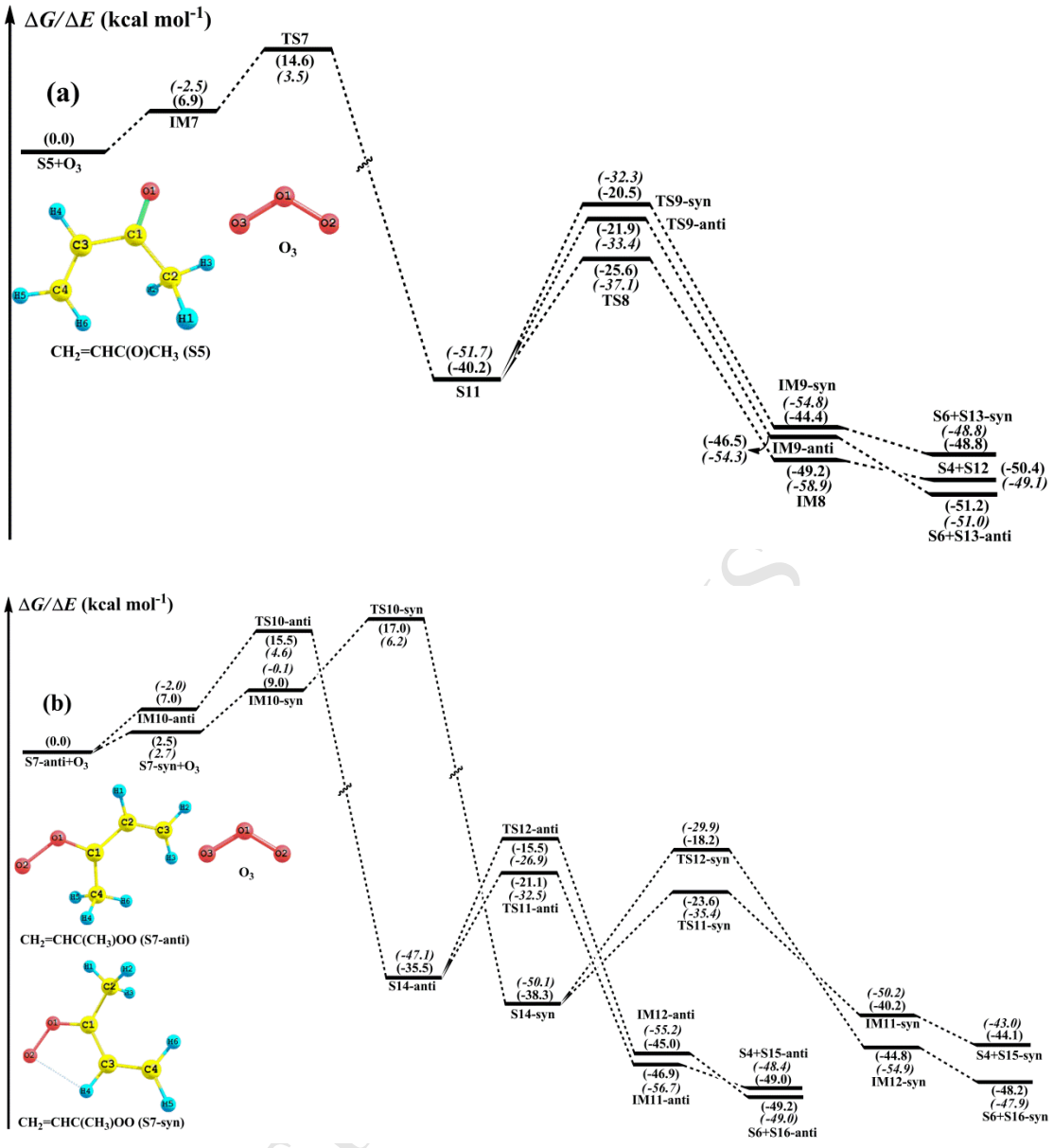
ΔG/ΔE (kcal mol-1)
(a)
(0.0)
S5+O3
(-2.5)
(6.9)
IM7
TS7
(14.6)
(3.5)
CH2=CHC(O)CH3 (S5)
O3
(-51.7)
(-40.2)
S11
(-32.3)
(-20.5)
TS9-syn
(-21.9)
(-33.4)
TS9-anti
(-25.6)
(-37.1)
TS8
IM9-syn
(-54.8)
(-44.4)
(-46.5)
(-54.3)
IM9-anti
(-49.2)
(-58.9)
IM8
S6+S13-syn
(-48.8)
(-48.8)
S4+S12
(-50.4)
(-49.1)
(-51.2)
(-51.0)
S6+S13-anti
ΔG/ΔE (kcal mol-1)
(b)
(0.0)
S7-anti+O3
(-2.0)
(7.0)
IM10-anti
(2.5)
(2.7)
S7-syn+O3
TS10-anti
(15.5)
(4.6)
(-0.1)
(9.0)
IM10-syn
TS10-syn
(17.0)
(6.2)
CH2=CHC(CH3)OO (S7-anti)
O3
CH2=CHC(CH3)OO (S7-syn)
(-47.1)
(-35.5)
S14-anti
TS12-anti
(-15.5)
(-26.9)
(-21.1)
(-32.5)
TS11-anti
(-50.1)
(-38.3)
S14-syn
(-29.9)
(-18.2)
TS12-syn
(-23.6)
(-35.4)
TS11-syn
IM12-anti
(-55.2)
(-45.0)
(-46.9)
(-56.7)
IM11-anti
S4+S15-anti
(-48.4)
(-49.0)
(-49.2)
(-49.0)
S6+S16-anti
(-50.2)
(-40.2)
IM11-syn
(-44.8)
(-54.9)
IM12-syn
(-43.0)
(-44.1)
S4+S15-syn
(-48.2)
(-47.9)
S6+S16-syn

Fig. 2

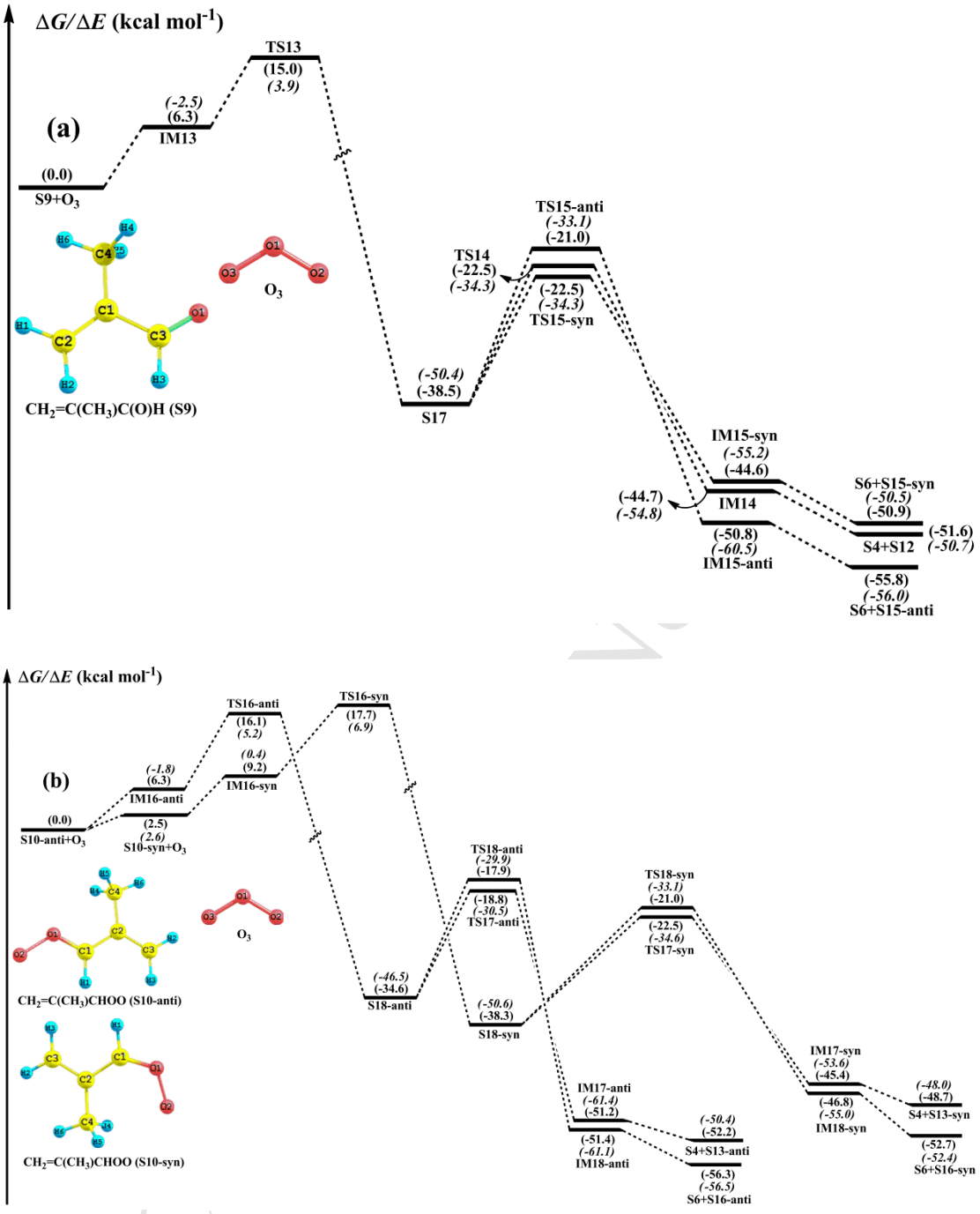
ΔG/ΔE (kcal mol-1)
(a)
TS13
(15.0)
(3.9)
(-2.5)
(6.3)
IM13
(0.0)
S9+O3
CH2=C(CH3)C(O)H (S9)
O3
TS15-anti
(-33.1)
(-21.0)
TS14
(-22.5)
(-34.3)
(-22.5)
(-34.3)
TS15-syn
(-50.4)
(-38.5)
S17
IM15-syn
(-55.2)
(-44.6)
(-44.7)
(-54.8)
IM14
(-50.8)
(-60.5)
IM15-anti
S6+S15-syn
(-50.5)
(-50.9)
(-51.6)
(-50.7)
S4+S12
(-55.8)
(-56.0)
S6+S15-anti
ΔG/ΔE (kcal mol-1)
(b)
TS16-anti
(16.1)
(5.2)
TS16-syn
(17.7)
(6.9)
(-1.8)
(6.3)
IM16-anti
(0.4)
(9.2)
IM16-syn
(0.0)
S10-anti+O3
(2.5)
(2.6)
S10-syn+O3
CH2=C(CH3)CHOO (S10-anti)
CH2=C(CH3)CHOO (S10-syn)
TS18-anti
(-29.9)
(-17.9)
(-18.8)
(-30.5)
TS17-anti
(-46.5)
(-34.6)
S18-anti
(-50.6)
(-38.3)
S18-syn
TS18-syn
(-33.1)
(-21.0)
(-22.5)
(-34.6)
TS17-syn
IM17-anti
(-61.4)
(-51.2)
(-51.4)
(-61.1)
IM18-anti
(-50.4)
(-52.2)
S4+S13-anti
(-56.3)
(-56.5)
S6+S16-anti
IM17-syn
(-53.6)
(-45.4)
(-46.8)
(-55.0)
IM18-syn
(-48.0)
(-48.7)
S4+S13-syn
(-52.7)
(-52.4)
S6+S16-syn

Fig. 3

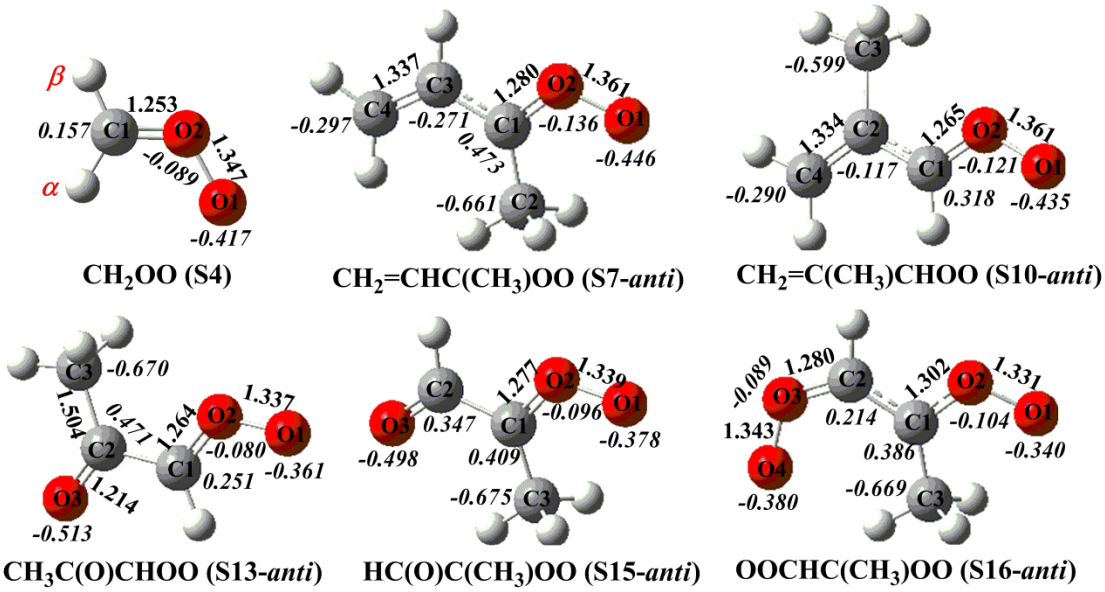

Fig. 4

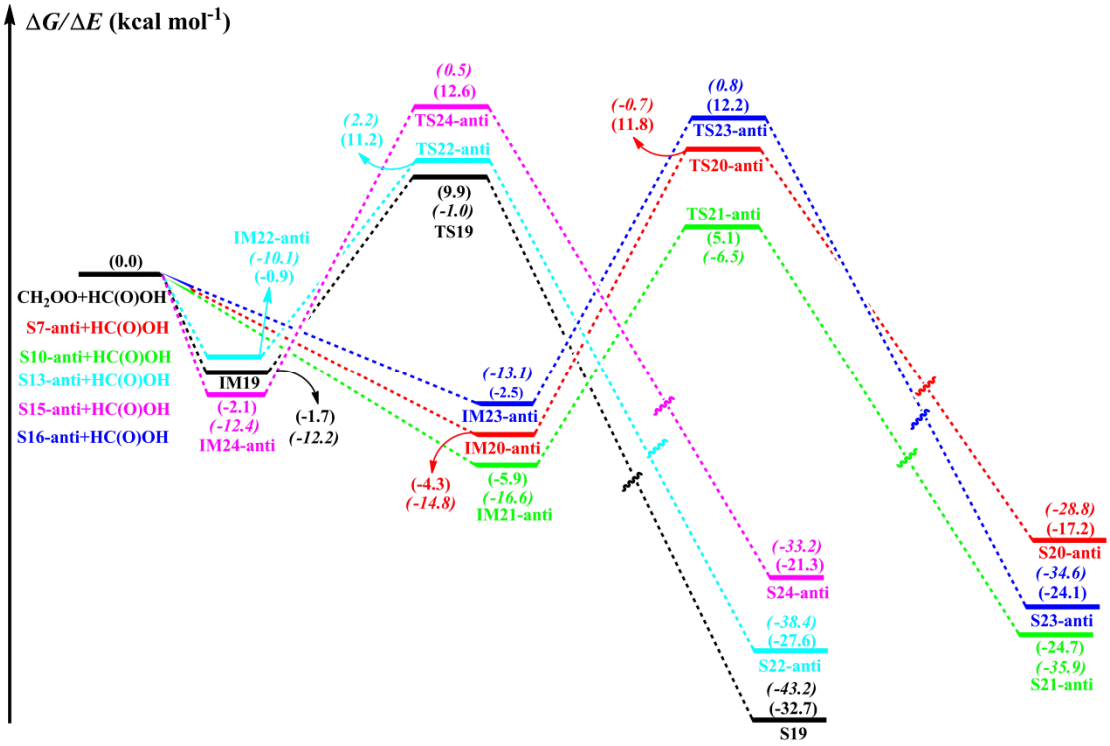

Fig. 5

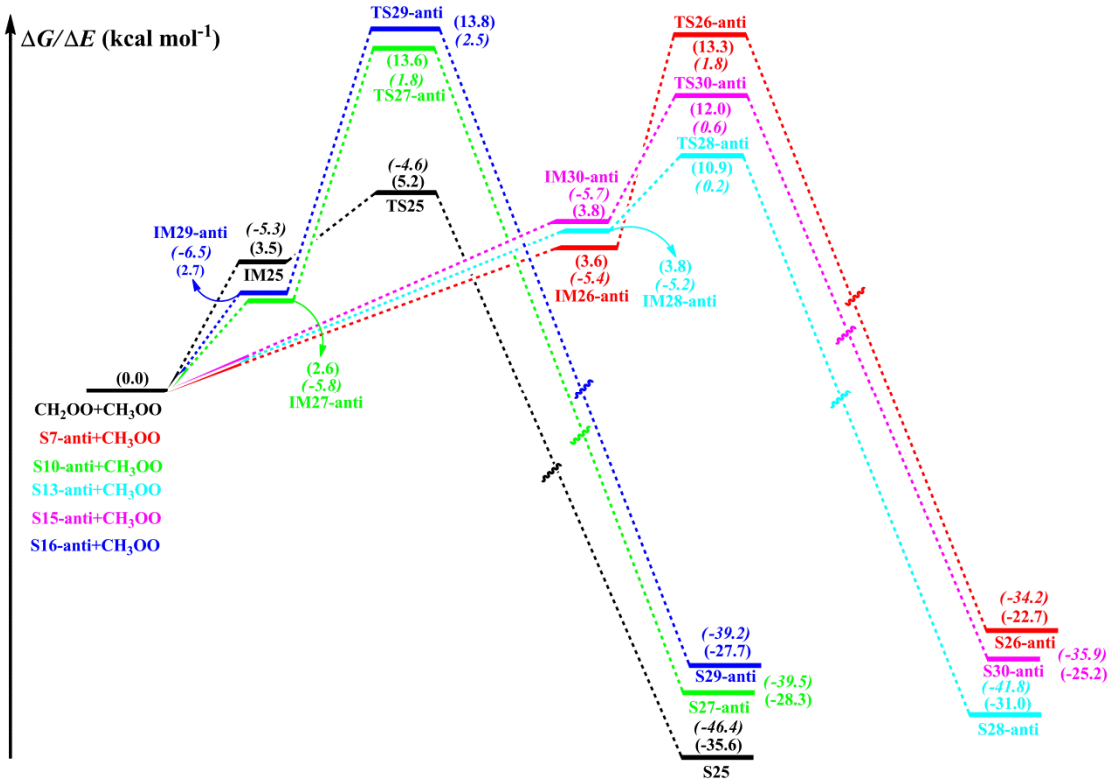

Fig. 6

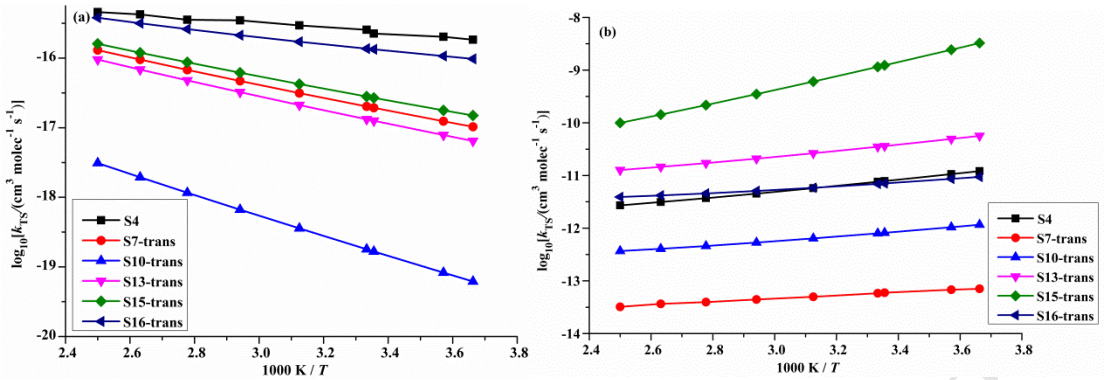

Fig. 7

Isoprene ozonolysis is one of the main atmospheric oxidation pathways forming SOA.

Theoretical calculations show that this process can produce various stable SCIs.

Reaction between SCIs and CH_3O_2 contributes significantly to the oligomer formation.

Oligomers containing a SCI as the chain units participate in SOA formation.

Such knowledge is useful for developing SOA atmospheric chemistry model.